

An improved process-oriented hydro-biogeochemical model for simulating dynamic fluxes of methane and nitrous oxide in alpine ecosystems with seasonally frozen soils

Wei Zhang¹, Zhisheng Yao¹, Siqi Li¹, Xunhua Zheng^{1, 2}, Han Zhang^{1, 3}, Lei Ma^{1, 4}, Kai Wang¹, Rui Wang¹, Chunyan Liu¹, Shenghui Han¹, Jia Deng⁵, Yong Li⁶

¹State Key Laboratory of Atmospheric Boundary Layer Physics and Atmospheric Chemistry, Institute of Atmospheric Physics, Chinese Academy of Sciences, Beijing 100029, P. R. China

²College of Earth and Planetary Science, University of Chinese Academy of Sciences, Beijing 100049, P. R. China

³School of Geographic and Environmental Sciences, Tianjin Normal University, Tianjin 300387, P. R. China

⁴Institute of Meteorology and Climate Research, Atmospheric Environmental Research (IMK-IFU), Karlsruhe Institute of Technology, Kreuzeckbahnstrasse 19, 82467 Garmisch-Partenkirchen, Germany

⁵Complex Systems Research Center, Institute for the Study of Earth, Oceans and Space, University of New Hampshire, 39 College Road, Durham, NH 03824, USA

⁶Key Laboratory of Agro-ecological Processes in Subtropical Region, Institute of Subtropical Agriculture, Chinese Academy of Sciences, Hunan 410125, P. R. China

Correspondence to: Xunhua Zheng (xunhua.zheng@post.iap.ac.cn)

Abstract. The hydro-biogeochemical model Catchment Nutrient Management Model - DeNitrification-DeComposition (CNMM-DNDC) was established to simultaneously quantify ecosystem productivity and losses of nitrogen and carbon at the site or catchment scale. As a process-oriented model, this model is expected to be universally applied to different climate zones, soils, land uses and field management practices. This study is one of many efforts to fulfil such an expectation, which was performed to improve the CNMM-DNDC by incorporating a physical-based soil thermal module to simulate the soil thermal regime in the presence of freeze-thaw cycles. The modified model was validated with simultaneous field observations in three typical alpine ecosystems (wetlands, meadows and forests) within a catchment located in the seasonally frozen region of the eastern Tibetan Plateau. Then, the model was further applied to evaluate its performance in simulating the effects of alpine wetland degradation on methane (CH₄) and nitrous oxide (N₂O) fluxes. The validation showed that the modified CNMM-DNDC was able to simulate the observed seasonal dynamics and magnitudes of soil temperature, topsoil moisture, and fluxes of CH₄ and N₂O in the three typical alpine ecosystems, with index of agreement values of 0.91–1.00, 0.49–0.83, 0.57–0.88 and 0.26–0.47, respectively. Consistent with the emissions determined from the field observations, the simulated aggregate emissions of CH₄ and N₂O were significantly reduced due to wetland degradation and were dominated by a reduction in CH₄ emissions. This study indicates the possibility for utilizing the process-oriented model CNMM-DNDC to predict hydro-biogeochemical processes, as well as related gas emissions, in seasonally frozen regions. As the original CNMM-DNDC was previously validated in some unfrozen regions, the modified CNMM-DNDC could be potentially

34 applied to estimate the emissions of CH₄ and N₂O from various ecosystems under different climate zones at the site or
35 catchment scale.

36 1 Introduction

37 During the last 50 years, the extraordinary changes in the nitrogen and carbon cycles have occurred globally, which are
38 essential components of ecosystems (e.g., Galloway *et al.*, 2008; Canfield *et al.*, 2010). Climate changes due to warming and
39 human anthropogenic activities derived from food production have significantly altered the cycling of nitrogen and carbon
40 and led to increased reactive nitrogen availability and carbon losses, which result in a series of environmental problems at
41 the catchment, regional and even global scales (e.g., Galloway *et al.*, 2004; Galloway *et al.*, 2008; Ju *et al.*, 2009). Excessive
42 reactive nitrogen in soils can be lost in the forms of nitrogen gases, such as nitrous oxide (N₂O), nitric oxide (NO) and
43 ammonia (NH₃), and nitrogen pollution, such as nitrate (NO₃⁻) and ammonium (NH₄⁺), in water through leaching or surface
44 runoff (e.g., Seitzinger, 2008; Collins *et al.*, 2016). In the face of increased air temperatures and intensive land use changes,
45 especially in cold regions, the soil organic carbon stored since the Last Glacial Maximum has been lost to the atmosphere via
46 methane (CH₄) and carbon dioxide (CO₂) (e.g., Piao *et al.*, 2009; Fenner and Freeman, 2011; Schuur *et al.*, 2015). These
47 nitrogen and carbon losses contribute to potential global warming (CO₂, CH₄ and N₂O), air pollution (NO and NH₃) and
48 surface/groundwater pollution (NO₃⁻ and NH₄⁺). Therefore, sustainable ecosystems urgently need to be established that not
49 only focus on net primary productivity but also are friendly to the environment with the minimal hazards, including
50 greenhouse gases, air pollution and water pollutants (e.g., Cui *et al.*, 2018; Zhang *et al.*, 2019).

51 The cycling of nitrogen and carbon is closely related to soil water processes (e.g., Breuer *et al.*, 2010; Vereecken *et al.*,
52 2016; Zhang *et al.*, 2018b). Thus, interactions among soil waters and the cycling of nitrogen and carbon govern biological
53 productivity and environmental outcomes (e.g., Zhu *et al.*, 2018). The interactions consist of the redox potential for different
54 transformation processes influenced by the spatiotemporal variation in soil water content and the lateral transport of water
55 and dissolved nitrogen or carbon controlled by surface and subsurface flow (e.g., McClain *et al.*, 2003; Castellano *et al.*,
56 2013; Bechmann, 2014). For example, the variation in soil water content can create hot spots or moments of nitrogen and
57 carbon losses by influencing plant nitrogen uptake, redox potential, and the transport of dissolved nitrogen and carbon (e.g.,
58 Zhu *et al.*, 2012; Keiluweit *et al.*, 2017). Therefore, a complete understanding of biogeochemical processes will inevitably
59 involve interactions among soil water and the cycling of nitrogen and carbon (e.g., Breuer *et al.*, 2010; Vereecken *et al.*,
60 2016; Zhu *et al.*, 2018).

61 Biogeochemical models, such as DNDC, LandscapeDNDC, WNMM, MOMOS, CENTURY and DayCent, are
62 effective tools for simulating the cycling of nitrogen and carbon and quantifying the effects of climate change and
63 anthropogenic activities on ecosystems (e.g., Foereid *et al.*, 2007; Haas *et al.*, 2012; Li, 2007; Li *et al.*, 2007; Pansu *et al.*,
64 2010; Cheng *et al.*, 2014; Pansu *et al.*, 2014). In recent years, some new conceptual approaches are applied in the
65 biogeochemical models, such as centering on the functional role of the soil microbial biomass (Pansu *et al.*, 2010; Pansu *et*

66 *al.*, 2014) and detailing the lateral transport of water and nutrients (Haas *et al.*, 2012; Zhang *et al.*, 2018b). Generally,
67 comprehensive hydrological processes, especially for the lateral transport of water and nutrients, are simplified or ignored in
68 most models due to specific questions that must be addressed (e.g., Li, 2007; Li *et al.*, 2007; Chen *et al.*, 2008; Deng *et al.*,
69 2014). For the land surface or hydrological models at large scales, they are designed with explicit mechanisms of hydrology
70 and generally focus on vertical and lateral nutrient transport, such as nitrate loads into rivers (e.g., Liu *et al.*, 2019). However,
71 the simulations of nitrogen and carbon processes are usually based on empirical functions even without predicting gas loss.
72 Due to the various purposes of different models, coupling soil hydrological models with biogeochemical models can be an
73 effective strategy for integrating soil water and cycling of nitrogen and carbon to improve model performance. Thus, the
74 coupled model with improved performance can be applied to simultaneously predict productivity and potential negative
75 environmental effects (e.g., Chen *et al.*, 2008; Zhu *et al.*, 2018).

76 In recent years, efforts have been implemented to couple models, such as SWAT-N, LandscapeDNDC-CMF, APSIM,
77 SWAT-DayCent, and CNMM-DNDC (e.g., Pohlert *et al.*, 2007; Haas *et al.*, 2012; Holzworth *et al.*, 2014; Wu *et al.*, 2016;
78 Zhang *et al.*, 2016; Zhang *et al.*, 2018b). The models derived from SWAT were all based on semi-distributed hydrological
79 models using hydrologic response units and did not perform better in estimating non-point source pollution (e.g., Pohlert *et al.*
80 *et al.*, 2007; Bosch *et al.*, 2011 ;Wu *et al.*, 2016). A coupler was used to couple two models for LandscapeDNDC-CMF, which
81 realized the simulation of horizontal movement of water and nutrients (e.g., Haas *et al.*, 2012; Klatt *et al.*, 2017; Schroeck *et al.*,
82 2019). Compared with other models, the Catchment Nutrient Management Model - DeNitrification-DeComposition
83 (CNMM-DNDC), which was established by incorporating the core biogeochemical processes of DNDC into the
84 hydrological framework of the CNMM, was validated at a catchment with complex landscapes in the subtropical region and
85 showed good performance for simultaneously simulating various variables, including ecosystem productivity, hydrological
86 nitrogen losses and nitrate discharge in streams, and emissions of gaseous carbon and nitrogenous gases (Zhang *et al.*,
87 2018b). Therefore, the CNMM-DNDC has the capacity to simulate the various variables closely related to both productivity
88 and environmental hazards.

89 However, as a process-oriented hydro-biogeochemical model designed to be applicable to different climate zones, soils,
90 land uses and field management practices, CNMM-DNDC testing is still lacking due to limited observations for model
91 validation. In this study, the model was applied to a catchment in a seasonally frozen region located on the eastern Tibetan
92 Plateau with the land use types of alpine wetlands, meadows and forests to test its ability to simulate hydro-biogeochemical
93 processes. However, scientific descriptions of soil thermal dynamics due to freeze-thaw cycles are still lacking for the
94 CNMM-DNDC. This gap may hinder model application in seasonally frozen regions, which account for 56% of the exposed
95 land surface of the Northern Hemisphere (Jiang *et al.*, 2020). In addition, the soil freeze-thaw cycles that occur in these mid-
96 high latitude regions exert important influences on soil thermal dynamics, as well as on related hydrological processes, thus
97 increasing the availability of substrates and stimulating the processes of CH₄ and N₂O production and emissions in soils (e.g.,
98 Song *et al.*, 2019). Therefore, we hypothesize that adding the missing scientific processes of soil thermal dynamics into the
99 internal model program codes can improve the performance of the CNMM-DNDC in simulating the soil thermal dynamics,

hydrological processes and CH₄ and N₂O fluxes in seasonally frozen regions. Filling this gap is especially necessary to broaden model applicability.

Nearly one-third of the wetlands in China are located in the Tibetan Plateau and more than 60% of those were fens (Gong *et al.*, 2010; Wei *et al.*, 2015). Due to intentional drainage for pasture enlargement during the past decades, more than 90% of the fens have degraded and turned to seasonally inundated or wet meadows (Wei *et al.*, 2015). This unprecedented large-scale land use change inevitably influences the exchange of CH₄ and N₂O fluxes at the soil-atmosphere boundary (e.g., Yao *et al.*, 2019; Zhang *et al.*, 2019; Zhang *et al.*, 2020). Zhang *et al.* (2019) found that intentional drainage has resulted in great reduction of CH₄ emissions. However, the nitrogen mineralization with falling water table for the degraded wetlands may increase the production N₂O (e.g., Hatano, 2019; Tan *et al.*, 2020; Zhang *et al.*, 2020). Therefore, we hypothesize that the CNMM-DNDC with improvements in soil thermal dynamics would have the potential to quantify the impacts of wetland degradation on CH₄ and N₂O fluxes.

To test the above hypothesis, the catchment simulation in the Rierlangshan was conducted using a unique experimental dataset, which was obtained by Zhang *et al.* (2018a, 2019) and Yao *et al.* (2019) for the catchment that involved three typical alpine ecosystems, wetlands, meadows and forests, on the eastern Tibetan Plateau. The aims of this study were to (i) attempt to address the gap in the CNMM-DNDC by improving the scientific processes of soil thermal dynamics for seasonally frozen regions; (ii) compare the performances of the original and modified models in simulating the soil profile temperature, topsoil moisture and CH₄ and N₂O fluxes in three typical alpine ecosystems in the Rierlangshan catchment with field observations, and (iii) quantifying the effects of wetland degradation on CH₄ and N₂O fluxes using the validated model. Therefore, the validated model with modifications provides a mechanism for not only interpreting observations but also predicting the CH₄ and N₂O fluxes in alpine ecosystems.

2 Materials and methods

2.1 Model description

2.1.1 Overview of the CNMM-DNDC model

The CNMM-DNDC is a process-oriented model developed for simulating hydro-biogeochemical interactions at the catchment or site scale, and this model is designed following the basic theories of physics, chemistry, and biogeochemistry and has the capacity to simulate the complex transport and transformation of water, nitrogen and carbon in terrestrial ecosystems under both aerobic and anaerobic conditions. The model can be applied to simultaneously quantify ecosystem productivity, net emissions of nitrogen and carbon gases and hydrological nitrogen losses through soil leaching and discharge in streams from an entire catchment or individual landscape unit (Zhang *et al.*, 2018b). The model was established to address the bottleneck issue associated with most biogeochemical models, i.e., the inability to simulate the lateral flows of water and nutrients, by incorporating the core biogeochemical processes of DNDC (including the processes of

decomposition, nitrification, denitrification and fermentation) into the hydrological framework of the CNMM, which is fully distributed. For the new generation of biogeochemical models, the microbial ecology was integrated into the biogeochemical models, which represents direct microbial control over decomposition, such as MOMOS (Pansu *et al.*, 2010; Treseder *et al.*, 2011; Todd-Brown *et al.*, 2012; Pansu *et al.*, 2014). The biogeochemical processes simulated by the DNDC were generally based on first-order kinetics for decomposition and Michaelis-Menten kinetics of two substrates for nitrification and denitrification, which only the parameterized growth and death of nitrifiers and denitrifiers were considered (Li, 2000). However, due to the global application and validation of DNDC (e.g., Chen *et al.*, 2008; Giltrap *et al.*, 2010; Cui *et al.*, 2014, Zhang *et al.*, 2015), the biogeochemical processes of DNDC were selected in the CNMM-DNDC despite some deficiencies in simulating microbial biomass.

The simulated soil depth (including bedrock) is user-defined. The temporal and spatial resolutions are also user-defined according to the driving data of climate (generally in 3 hours) and digital elevation model (DEM). The soil moisture was calculated based on the mass balance of precipitation, irrigation, evapotranspiration, vertical flow, lateral flow and water from a rising water table. The total water that can be infiltrated during each time step was determined by a defined maximum infiltration rate. Darcy's law was applied for predicting the vertical water flow in the soil profile. A cell-by-cell approach using a kinematic approximation was applied to route the saturated overland and subsurface flow based on DEM. The stream flow was estimated using a cascade of linear channel reservoirs (Wigmosta *et al.*, 1994). For plant growth, gross primary production was simulated using Farquhar *et al.* (1980) for C_3 and Collatz *et al.* (1992) for C_4 , with annual primary productivity calculated as the residue of gross primary production and autotrophic respiration. The processes related to the production of N_2O include nitrification and denitrification, which occur simultaneously at aerobic and anaerobic microsites, respectively. The concept of an "anaerobic balloon" was adopted to determine the microsites and allocate substrates for nitrification and denitrification. The sizes of the aerobic (nitrification) and anaerobic (denitrification) microsites were determined by the soil redox potential (Eh) using the Nernst equation (Li, 2007). The "hole in the pipe" concept was applied to calculate N_2O production during nitrification, which is influenced by the soil moisture, temperature and pH (Li, 2016). The production of N_2O during denitrification was predicted with Michaelis-Menten kinetics and Pirt functions following the reaction chain of denitrification. The predicted CH_4 flux was influenced by CH_4 production, oxidation and transportation derived from the module of fermentation in the DNDC (Li, 2007). Methane production and oxidation occurred simultaneously and were determined by the sizes of the aerobic (production) and anaerobic (oxidation) microsites, which were defined by an Eh calculator in terms of an "anaerobic balloon" (" CH_4 balloon") (Li, 2007). The predicted CH_4 production was calculated from the carbon substrates resulting from decomposed soil organic carbon (SOC) and plant root biomass with the effects of soil temperature (Li, 2000, 2016). For more details, please see Li. (2000, 2007) and Zhang *et al.* (2018b).

162 2.1.2 Modifications of the CNMM-DNDC model

163 In the CNMM-DNDC, the soil temperature was predicted by solving the one-dimensional heat conduction equation
 164 with the implicit method of Crank-Nicholson. However, despite the simple parameterization used for the calculation of soil
 165 heat capacity and thermal conductivity, the variations of soil temperature induced by the freeze-thaw cycles were also not
 166 considered (Table S1 of the online supplementary materials), which inevitably hindered its application in seasonally frozen
 167 regions. In this study, the CNMM-DNDC was modified by replacing the above soil thermal module by a physical based
 168 module of Northern Ecosystem Soil Temperature (Zhang *et al.*, 2003; Deng *et al.*, 2014), which can explicitly describe the
 169 energy exchange within the soil, the active layer dynamics and the soil thermal regime in the presence of freeze-thaw cycles.
 170 These modifications are indispensable for accurately simulating freeze-thaw cycles in seasonally frozen regions, which are
 171 crucial for characterizing the active layer and soil thermal dynamics, soil hydrology and nitrogen or carbon cycling in these
 172 regions. Therefore, the CNMM-DNDC with and without the above modifications are hereafter referred to as the original and
 173 modified model, respectively.

174 The modified thermal dynamics of the soil are calculated by the one-dimensional heat conduction equation (Eq. 1).
 175 The equation is solved numerically by converting to an explicit form (Eqs. 2–4), which is more efficient for considering the
 176 freeze-thaw cycles (Zhang *et al.*, 2003). In the above equations, C ($\text{J m}^{-3} \text{ }^{\circ}\text{C}^{-1}$), k ($\text{W m}^{-1} \text{ }^{\circ}\text{C}^{-1}$), T ($^{\circ}\text{C}$) and G (W m^{-2}) denote
 177 the soil heat capacity, thermal conductivity, soil temperature and heat fluxes between layers, respectively. Both Z and D are
 178 the thicknesses of the soil layer (m), Δt is the time step of the calculation, and l denotes the soil layer l . S is the internal heat
 179 exchange due to freezing or thawing (W m^{-3}) when the soil temperature is around $0 \text{ }^{\circ}\text{C}$. The soil temperature changes
 180 affected by freezing or thawing are determined on the basis of energy conservation, which indicate that the latent heat
 181 released during freezing equalled the amount of heat required for the increased soil temperature and vice versa. The dynamic
 182 soil heat capacity (C_l , $\text{J m}^{-3} \text{ }^{\circ}\text{C}^{-1}$) is the weighted average of the heat capacity for five constituents, including organic matter
 183 ($C_{l, \text{OM}}$), minerals ($C_{l, \text{Min}}$), water ($C_{l, \text{Water}}$), ice ($C_{l, \text{Ice}}$) and air ($C_{l, \text{Air}}$) (Eq. 5). The values of heat capacity for organic matter,
 184 minerals, water, ice and air were 2.5×10^6 , 2.0×10^6 , 4.2×10^6 , 2.1×10^6 and $1.2 \times 10^3 \text{ J m}^{-3} \text{ }^{\circ}\text{C}^{-1}$, respectively (Huang, 2000). The
 185 weight is the relative volumetric fraction of each constituent ($\theta_{l, \text{OM}}$, $\theta_{l, \text{Min}}$, $\theta_{l, \text{Water}}$, $\theta_{l, \text{Ice}}$, $\theta_{l, \text{Air}}$) in the soil. The dynamic
 186 thermal conductivity (k_l , $\text{W m}^{-1} \text{ }^{\circ}\text{C}^{-1}$) is calculated using the thermal conductivities of above five constituents (Eq. 6–13),
 187 with values of 0.25 ($k_{l, \text{OM}}$), 2.9 ($k_{l, \text{Min}}$), 0.57 ($k_{l, \text{Water}}$), 2.2 ($k_{l, \text{Ice}}$) and 0.025 ($k_{l, \text{Air}}$) $\text{W m}^{-1} \text{ }^{\circ}\text{C}^{-1}$ for organic matter, minerals,
 188 water, ice and air, respectively (Johansen, 1975). ST_l denotes the soil temperature of layer l ($^{\circ}\text{C}$). The upper and lower
 189 boundary conditions of the thermal dynamics were determined by the surface energy balance and the defined geothermal
 190 heat flux at a soil depth of 35 m.

$$C \frac{\partial T}{\partial t} = \frac{\partial}{\partial Z} \left(k \frac{\partial T}{\partial Z} \right) + S \quad (1)$$

$$C_l \frac{\Delta T_l}{\Delta t} = \frac{G_{l-1, l} - G_{l, l+1}}{D_l} + S_l \quad (2)$$

$$G_{l-1,l} = \frac{(0.5k_l + 0.5k_{l-1})(T_{l-1} - T_l)}{0.5D_{l-1} + 0.5D_l} \quad (3)$$

$$G_{l,l+1} = \frac{(0.5k_l + 0.5k_{l+1})(T_l - T_{l+1})}{0.5D_l + 0.5D_{l+1}} \quad (4)$$

$$C_l = C_{l,OM}\theta_{l,OM} + C_{l,Min}\theta_{l,Min} + C_{l,Water}\theta_{l,Water} + C_{l,Ice}\theta_{l,Ice} + C_{l,Air}\theta_{l,Air} \quad (5)$$

$$k_l = \frac{\theta_{l,Water}k_{l,Water} + F_{l,Air}\theta_{l,Air}k_{l,Air_adj} + F_{l,OM+Min}(\theta_{l,OM} + \theta_{l,Min})k_{l,OM+Min} + F_{l,Ice}\theta_{l,Ice}k_{l,Ice}}{\theta_{l,Water} + F_{l,Air}\theta_{l,Air} + F_{l,OM+Min}(\theta_{l,OM} + \theta_{l,Min}) + F_{l,Ice}\theta_{l,Ice}} \quad (6)$$

$$k_{l,Air_adj} = \begin{cases} k_{l,Air} + 0.0238e^{0.0536ST_l} & (\theta_{l,Water} > 0.09) \\ 0.418 \times (0.0615 + 1.96\theta_{l,Water}) & (\theta_{l,Water} \geq 0.09) \end{cases} \quad (7)$$

$$g_a = \begin{cases} 0.333 - \frac{0.298\theta_{l,Air}}{1 - \theta_{l,OM} - \theta_{l,Min}} & (\theta_{l,Water} > 0.09) \\ 0.013 + 0.944\theta_{l,Water} & (\theta_{l,Water} \geq 0.09) \end{cases} \quad (8)$$

$$g_c = 1.0 - 2.0g_a \quad (9)$$

$$k_{l,OM+Min} = k_{l,OM} \frac{\theta_{l,OM}}{\theta_{l,OM} + \theta_{l,Min}} + k_{l,Min} \frac{\theta_{l,Min}}{\theta_{l,OM} + \theta_{l,Min}} \quad (10)$$

$$F_{l,Air} = 0.333 \left(\frac{2.0}{1.0 + g_a \left(\frac{k_{l,Air_adj}}{k_{l,Water}} - 1.0 \right)} + \frac{1.0}{1.0 + g_c \left(\frac{k_{l,Air_adj}}{k_{l,Water}} - 1.0 \right)} \right) \quad (11)$$

$$F_{l,OM+Min} = 0.333 \left(\frac{2.0}{1.0 + 0.125 \left(\frac{k_{l,OM+Min}}{k_{l,Water}} - 1.0 \right)} + \frac{1.0}{1.0 + 0.75 \left(\frac{k_{l,OM+Min}}{k_{l,Water}} - 1.0 \right)} \right) \quad (12)$$

$$F_{l,Ice} = 0.333 \left(\frac{2.0}{1.0 + 0.125 \left(\frac{k_{l,Ice}}{k_{l,Water}} - 1.0 \right)} + \frac{1.0}{1.0 + 0.75 \left(\frac{k_{l,Ice}}{k_{l,Water}} - 1.0 \right)} \right) \quad (13)$$

191

192 Compared to the original thermal module, the internal heat exchange due to freezing or thawing (S) was included with
 193 improved algorithm for thermal conductivity (k). In addition, the one-dimensional heat conduction equation (Eq. 1) was
 194 solved by converting it to an explicit form in the modified model (Eqs. 2–4), while was solved with the implicit method in
 195 the original models (Table S1). The modified CNMM-DNDC was able to simulate the thermal dynamics in seasonally
 196 frozen regions as well as their impacts on biogeochemical processes, such as the emissions of nitrogen and carbon gases.

197 2.2 Catchment and field descriptions

198 The study area is the Rierlangshan catchment (34°02'N, 102°43'E) on the eastern Tibetan Plateau with an area of 189
 199 ha (Yao *et al.*, 2019). This catchment is located in the source region of the Pai-Lung River, which is a sub-branch of the
 200 upper Yangtze River (Zhang *et al.*, 2018a; 2019). This region is subject to a cold humid continental monsoon climate, and it

201 had an annual mean air temperature of 1.6 ± 0.7 °C and average annual precipitation of 649 ± 94 mm in 1980–2012 as
202 observed at the Zoige Meteorological Station (~80 km south of the catchment) (Ma *et al.*, 2018). The catchment consists of
203 alpine wetlands, meadows and forests (Yao *et al.*, 2019). The alpine wetlands in the catchment are part of the Zoige wetland
204 and are degraded due to anthropogenic drainage and climate warming (Dong *et al.*, 2010; Li *et al.*, 2014). Degraded alpine
205 wetlands are commonly distributed throughout the Zoige wetland, and nearly 83% of the permanently inundated wetlands
206 have been converted into “wet grassland” (Xiang *et al.*, 2009; Li *et al.*, 2014).

207 CH₄ and N₂O fluxes were manually measured weekly or twice per week using the gas chromatograph-based static
208 opaque chamber method (Zhang *et al.*, 2018a) at three sites in alpine wetlands (34°02′6.53″N, 102°43′29.66″E, 3304 m
209 a.s.l.), meadows (34°02′01″N, 102°43′28″E, 3326 m a.s.l.) and forests (34°01′47.13″N, 102°44′0.87″E, 3415 m a.s.l.) in the
210 Rierlangshan catchment from 2013 to 2015 (Zhang *et al.*, 2018a; Yao *et al.*, 2019; Zhang *et al.*, 2019) (Fig. S1). Each
211 chamber was wrapped with a layer of styrofoam and aluminium foil to mitigate temperature increases inside the enclosures
212 due to the heating of solar radiation. The alpine wetland site is located at a slope base with a slope of 2°. The wetland has
213 suffered from anthropogenic drainage and climate warming, and thus degraded to be seasonally inundated. The alpine
214 meadow site neighbours the alpine wetland site, which is located on the north-facing slope with gradient of 11°. In addition,
215 soil temperatures at different depths and topsoil moisture in the alpine wetlands, meadows and forests were observed daily
216 and twice per week, respectively. The details regarding the available field observations of the CH₄ and N₂O fluxes and the
217 relevant auxiliary variables are described in Table S2.

218 2.3 Model simulation

219 The modified CNMM-DNDC was applied in the Rierlangshan catchment with the three alpine ecosystems: wetlands,
220 meadows and forests. The dataset required for the catchment simulation included (1) a digital elevation model (DEM) with a
221 resolution of 30×30 m² from the geospatial data cloud (Fig. S1; <http://www.gscloud.cn/>); (2) a map of alpine ecosystems,
222 including wetlands, meadows and forests; (3) a climate dataset of 3-hour weather data (air temperature, precipitation, wind
223 speed, solar radiation, longwave radiation, and humidity), which were obtained from the meteorological station in the target
224 catchment for the years with field observations (2013.11–2015.10) and were adapted from the daily data at the Zoige
225 Meteorological Station (provided by the National Meteorological Information Center: <http://data.cma.cn/>; last access: 10th
226 June, 2020) for other years; (4) a soil properties dataset of the observed clay fraction, organic matter content, total nitrogen,
227 pH and bulk density of the three alpine ecosystems in 1 m soil profile (Ma *et al.*, 2018; Zhang *et al.*, 2018a; Yao *et al.*, 2019;
228 Zhang *et al.*, 2019; Table S3); and (5) a management practices dataset including grazing time and intensity for the alpine
229 wetlands and meadows (Table S3). In addition, other required soil inputs of field capacity, wilting point and saturated
230 hydrological conductivity were calculated by pedo-transfer functions (Li *et al.*, 2019; Table S4). The simulated soil depth
231 was defined as 35 m due to the lower boundary conditions of the thermal dynamics, which was set as the geothermal heat
232 flux at a soil depth of 35 m. The simulated soil profile (0–35 m depth) was divided into 23 layers, including the soil (0–1.5
233 m) and bedrock (1.5–35 m). The layer thicknesses of the soil (0–1.5 m) were 1, 5, 10 and 50 cm for the depth of 0–10, 10–20,

234 20–100 and 100–150 cm, respectively. The layer thicknesses of the bedrock (1.5–35 m) were 3.5 and 31m for the depth of
235 1.5–4.0 and 4.0–35 m, respectively. The geothermal heat flux in the catchment was estimated at 0.053 W m^{-2} (Pollack and
236 Chapman, 1977). For the target catchment, the soil water dynamics of the alpine ecosystems were determined by the
237 precipitation, evapotranspiration, infiltration, penetration and lateral flow. Using the database, a catchment simulation of
238 hydro-biogeochemical processes was performed with spatial and temporal resolutions of $30 \times 30 \text{ m}^2$ and 3 hours, respectively,
239 by the modified CNMM-DNDC from 2012 to 2015, which could reflect the influences of hydrological processes on soil
240 water dynamics. Thus, the soil water dynamics of the seasonally inundated wetlands were determined by the hydrological
241 processes without any artificial disturbances in the catchment simulation.

242 In order to quantify the effects of wetland degradation on CH_4 and N_2O fluxes by the validated model, a scenario
243 simulation for the annually inundated wetland was performed at the catchment scale through arbitrarily setting the minimal
244 water table of the validated alpine wetland as 5 cm.

245 2.4 Statistics and analysis

246 The statistical criteria applied for evaluating the model performance in this study included (i) the index of agreement
247 (IA), (ii) the Nash–Sutcliffe index (NSE), and (iii) the determination coefficient (R^2) and slope of the zero-intercept
248 univariate linear regression (ZIR) of the observations against the simulations (e.g., Nash and Sutcliffe, 1970; Willmott and
249 Matsuura, 2005; Moriasi *et al.*, 2007; Congreves *et al.*, 2016; Jiang, 2010; Dubache *et al.*, 2019). A value of IA (0–1) closer
250 to 1 showed a better simulation. An NSE value (ranging from minus infinity to 1) closer to 1 was better. Better model
251 performance was indicated by a slope and an R^2 value that were both closer to 1 in a significant ZIR. For more details on
252 these criteria, refer to the Eqs. S1–4 in Table S5. In addition, the SPSS Statistics Client 19.0 (SPSS Inc., Chicago, USA) and
253 Origin 8.0 (OriginLab, Northampton, MA, USA) software packages were applied for the statistical analysis and graphical
254 comparison.

255 3 Results

256 3.1 Model validation

257 3.1.1 Soil temperature and moisture

258 The profile soil temperatures were observed for alpine wetland and meadow, but only topsoil temperature was
259 observed for the alpine forest, which could be used for model validation. The simulated soil temperatures of the three typical
260 alpine ecosystems were significantly improved by including the scientific processes of soil thermal dynamics suitable for
261 seasonally frozen regions (Figs. 1 and S2). The simulated seasonal dynamics and magnitudes were consistent with those
262 from the field observations for various soil depths, with IA, NSE, and ZIR slopes and R^2 values of 0.91–1.00, 0.68–0.99,
263 0.83–1.09 and 0.73–1.00 for the three alpine ecosystems, respectively (Table 1). For the observed alpine wetlands and

meadows, the simulation showed that the freezing of soil started in early November and continued to the end of April in the next year. The frozen depth reached a maximum in the middle of February. However, the simulated maximum frozen depths for the observed alpine meadows (0.69–0.74 m) were approximately double those for the alpine wetlands (0.30–0.39 m) (Fig. S3).

For the soil moisture, only topsoil moisture was observed in the three alpine ecosystems, which could be applied for model validation. The simulated topsoil moisture dynamics were comparable to those from the field observations, with IA and NSE values of 0.49–0.83 and -0.80–0.32 for the three alpine ecosystems, respectively (Fig. 2 and Table 1). In comparison to the other alpine ecosystems, the alpine wetlands had higher soil moisture, which ranged from 0.41 to 0.98 and from 0.38 to 0.93 for the observations and simulations in the water-filled pore space (WFPS), respectively. The soil moisture values of the alpine meadows and forests were highly variable and depended on the variation trend in precipitation for both observations and simulations. However, an underestimation of soil moisture in the winter period occurred for both alpine meadows and forests due to a possible overestimation of evapotranspiration. The performances of the modified model in simulating the soil profile temperature and topsoil moisture indicate that the modified CNMM-DNDC can generally predict the soil thermal and topsoil moisture dynamics in the three alpine ecosystems, which is crucial for correctly simulating soil hydrology, plant growth and biogeochemical processes.

3.1.2 Methane fluxes

The daily observed CH₄ emissions from the alpine wetlands were highly variable and showed a clear seasonal cycle, with intensive CH₄ emissions from May to November and weak emissions in other periods (Fig. 3a). The observed alpine meadows and forests functioned exclusively as sinks of atmospheric CH₄ with higher rates of uptake during the growing season and lower uptake rates in the dormant season (Figs. 3b–c). The original model significantly overestimated CH₄ emissions from the alpine wetlands. The modified CNMM-DNDC accurately identified the functions of the sources or sinks in the three alpine ecosystems and generally captured the magnitude and seasonal characteristics of the daily CH₄ fluxes, with an IA of 0.57–0.88 for the three alpine ecosystems (Figs. 3 and Table 1). However, the CH₄ uptake rates during the dormant season were obviously underestimated by the modified model at both sites, especially at the alpine forest site, which was responsible for the underestimation of cumulative CH₄ uptake. The observed cumulative CH₄ emissions ranged from -2.60 to 33.5 kg C ha⁻¹ yr⁻¹ and the modelled values ranged from -1.90 to 31.0 kg C ha⁻¹ yr⁻¹ (Fig. 6a). For the catchment simulation, the simulated annual CH₄ emissions ranged from -2.35 to 73.0 kg C ha⁻¹ yr⁻¹ from November 2013 to November 2014 (Fig. S4a). These results indicate that the modified CNMM-DNDC well simulated the CH₄ fluxes of the three typical alpine ecosystems.

3.1.3 Nitrous oxide fluxes

The daily observed N₂O emissions from the alpine wetlands were higher than those from the alpine meadows but lower than those from the alpine forests (Figs. 3b, 4b and 5b). Similar seasonal patterns of N₂O fluxes were observed for the

three alpine ecosystems with intensive emissions in the growing season. The N₂O emission peak during the dormant season was observed in the alpine meadows, which was the major contributor to annual emissions. The modified CNMM-DNDC generally captured the seasonal dynamics of daily N₂O fluxes with an IA of 0.26–0.47 for the three alpine ecosystems (Figs. 3d–f and Table 1), but the N₂O emissions from the alpine wetlands were significantly overestimated by the original model. For the modified model, the simulated N₂O emissions from the alpine wetlands and forests showed obvious seasonal patterns with higher emissions during the growing season, but no abrupt emission peak was captured at the end of the growing season for the alpine wetlands. In addition, compared with the original model, the modified model captured the peak emissions that occurred during the freeze-thaw period from the alpine meadows due to the death of microbes, but the dynamics of the peak emissions were not well simulated. The observed cumulative N₂O emissions ranged from 0.14 to 0.58 kg N ha⁻¹ yr⁻¹ and the modelled values ranged from 0.12 to 0.32 kg N ha⁻¹ yr⁻¹ (Fig. 6b). For the catchment simulation, the simulated annual N₂O emissions ranged from 0.01 to 0.74 kg N ha⁻¹ yr⁻¹ from November 2013 to November 2014 (Fig. S4b). These results indicate that the modified CNMM-DNDC has the potential to estimate N₂O emissions in seasonally frozen regions.

3.2 Annual aggregate emissions of CH₄ and N₂O

Annual aggregate emissions of CH₄ and N₂O in carbon dioxide (CO₂) equivalents were calculated for the three alpine ecosystems from November 2013 to November 2014 for alpine wetlands and meadow and from April 2014 to April 2015 for alpine forests, and the global warming potentials were 34 for CH₄ and 298 for N₂O on a 100-year time horizon (IPCC, 2013). The simulated aggregate emissions by the modified model were 1.5, 0.015, and 0.061 Mg CO₂eq ha⁻¹ yr⁻¹ for the observed alpine wetlands, meadows and forests, respectively, which were consistent with those from the field observations (1.6, 0.014, and 0.15 Mg CO₂eq ha⁻¹ yr⁻¹ for the alpine wetlands, meadows and forests, respectively) (Fig. 4c). However, the original model significantly overestimated the aggregate emissions due to the high predicted CH₄ and N₂O emissions. In comparison, the observed seasonally inundated wetlands functioned as the sources of aggregate emissions of CH₄ and N₂O, but the aggregate emissions from adjacent wet alpine meadows were much lower.

For the scenario simulation of annually inundated wetlands, the simulated aggregate emissions of CH₄ and N₂O were 7.2 Mg CO₂eq ha⁻¹ yr⁻¹ with CH₄ and N₂O emissions of 158 kg C ha⁻¹ yr⁻¹ and 0.0 kg N ha⁻¹ yr⁻¹, respectively (Fig. 4). The simulation indicates that wetland degradation resulted in decreased CH₄ emissions but increased N₂O emissions. However, the increased N₂O emissions could be totally offset by the reduced CH₄ emissions, thus finally leading to the decreased aggregate emissions of CH₄ and N₂O from degraded wetlands than permanently inundated wetlands but still much higher than those of adjacent wet alpine meadows.

324 4 Discussions

325 4.1 Model performance in simulating thermal dynamics

326 The soil freeze-thaw cycles in seasonally frozen regions determine the soil profile temperature and hydrological
327 processes, which are key factors that regulate the cycling of nitrogen and carbon (e.g., Zhang *et al.*, 2015; Hugelius *et al.*,
328 2020). Therefore, improving the scientific processes of soil thermal dynamics in the presence of active layer dynamics is
329 essential for applying the CNMM-DNDC to simulate the biogeochemical processes in seasonally frozen regions, which are
330 sensitive and vulnerable to climate change and human activities (Hatano, 2019; Hugelius *et al.*, 2020; Jiang *et al.*, 2020). The
331 original model adopted a relatively simple module to calculate thermal transportation within the soil profile and did not
332 consider the effects of freeze-thaw cycles on soil temperature and moisture. The newly incorporated module was based on
333 explicit energy conservation and exchange in the soil profile and successfully captured the variations in soil temperature and
334 topsoil moisture for the three alpine ecosystems during the freeze-thaw period. The simulated lower soil frozen depth for the
335 observed alpine wetland was primarily attributed to the higher soil profile moisture level, as the thermal conductivity and
336 heat capacity for water-filled pores were higher than those for air-filled pores. In order to quantify the impacts of climate
337 change on the cycling of carbon and water on the regional and global scales, several large scale ecosystem models or
338 macroscale hydrological models, such as Terrestrial Ecosystem Model, Lund-Potsdam-Jena dynamic global vegetation
339 model and Variable Infiltration Capacity model, have been enhanced to simulate the soil thermal dynamics at northern high
340 latitude (e.g., Wania *et al.*, 2009; Zhuang *et al.*, 2001; Cuo *et al.*, 2015; Jiang *et al.*, 2020). In addition, the soil thermal
341 modules were also improved in some biogeochemical models, such as DNDC and Mobile-DNDC, to evaluate the influences
342 of climate warming on the biogeochemical processes in high latitude regions (e.g., Zhang *et al.*, 2003; de Bruijn *et al.*, 2009;
343 Wolf *et al.*, 2011; Zhang *et al.*, 2012; Deng *et al.*, 2014). Compared with the simulated soil profile temperatures by above
344 models at different scales, the simulations in this study by the modified CNMM-DNDC were equally well, especially for
345 deeper soil layers (e.g., Wania *et al.*, 2009). For the validated topsoil moisture in this study, the modified model generally
346 captured the variation trends, which were comparable with the performances of other models (e.g., de Bruijn *et al.*, 2009;
347 Wolf *et al.*, 2011; Cuo *et al.*, 2015). However, compared with the studies focused on simulating soil moisture (e.g., Ford *et al.*,
348 2014), further improvements are still required to improve the model performance in simulating the soil moisture. These
349 results indicate the efficiency of the incorporated module in simulating soil thermal and topsoil moisture dynamics in
350 seasonally frozen regions.

351 4.2 Model performance in simulating CH₄ fluxes

352 Compared with the annually inundated wetlands, the seasonally inundated wetlands had relatively low observed and
353 simulated CH₄ emissions due to the significant influences of the water table level on CH₄ emissions (e.g., Hatano, 2019;
354 Zhang *et al.*, 2019). The CH₄ emissions simulated by the CNMM-DNDC were determined by the processes of production,
355 oxidation and transpiration. The unsaturated soil with moisture levels ranging from 0.41 to 0.98 WFPS resulted in a small

CH₄ balloon and thus reduced CH₄ production. At the same time, relatively dry conditions caused the upper soil layer to act as an efficient oxidative methanotrophic barrier for the diffusion of CH₄ from the subsoil and thus decreased CH₄ emissions (Kandel *et al.*, 2018; Tan *et al.*, 2020). In addition, the highly fluctuating CH₄ emissions simulated by the modified model were also attributed to the high dependency of CH₄ production on soil moisture, which controlled the size of the CH₄ balloon. Theoretically, the CH₄ emissions simulated by the original model should not be higher than those simulated by the modified model due to the lower predicted soil moisture level. The overestimated CH₄ emissions simulated by the original model were mainly attributed to the overestimated soil temperature due to their influences on mineralized substrates for CH₄ production, as well as the processes of CH₄ production. This result implies that global warming may trigger intensive CH₄ emissions from degraded wetlands, which could partly serve as a trade-off for the decreased CH₄ emissions due to the lower water table level in degraded wetlands (e.g., Gong *et al.*, 2020). For the studies focused on simulating CH₄ emissions from wetlands by the large-scale ecosystem models, the model validation with field observation is difficult due to coarse spatial resolution (e.g., Zhuang *et al.*, 2004). For the biogeochemical model, such as DNDC, the dynamics of CH₄ emissions from wetland and peatland in the northern permafrost regions were well simulated (Zhang *et al.*, 2012; Deng *et al.*, 2014), which showed consistent seasonal variations and magnitudes as those in this study. Both observations and simulations showed that the CH₄ uptake in alpine forests was higher than that in alpine meadows, which was mainly attributed to the high SOC content of the alpine forests in the simulation. Methane uptake by upland soils is a biological process governed by the availability of CH₄ and oxygen as well as the activity and quantity of methanotrophic bacteria in soils (e.g., Liu *et al.*, 2007; Zhang *et al.*, 2014). In the model, the simulated CH₄ uptake was positively related to the SOC content, which is closely related to the population size of methanotrophic bacteria. Thus, the SOC content primarily contributed to the differences in CH₄ uptake from alpine meadows and forests, as the values for forests were more than twice of those for meadows (Table S3). As the simulated dynamic characteristics of CH₄ uptake were primarily regulated by soil temperature and moisture, the inhibitory effects of low soil temperature (< 0.0 °C) on CH₄ uptake rates resulted in obvious underestimations in the dormant season for both alpine meadows and forests. Therefore, an improved parameterization for simulating CH₄ uptake under low soil temperatures is required for the model to better capture the dynamics of CH₄ uptake in the dormant season.

4.3 Model performance in simulating N₂O fluxes

In comparison, the N₂O emissions from the alpine wetlands and forests were higher than those from the alpine meadows for both the observations and simulations due to the high SOC content and nitrogen availability. Natural wetlands are large carbon reserves and play a crucial role in mitigating global warming (e.g., Deng *et al.*, 2014; Kang *et al.*, 2020; Tan *et al.*, 2020). The intentional drainage of annually inundated wetlands alters not only the water regime but also nutrient availability (e.g., Hoffmann *et al.*, 2016). The simulated relatively low soil moisture for the alpine wetlands stimulated the decomposition of SOC and nitrogen (or peat oxidation) under aerobic conditions, thus improving nitrogen mineralization for nitrification and denitrification and enhancing N₂O emissions (e.g., Tan *et al.*, 2020; Zhang *et al.*, 2020). The intensive N₂O emissions simulated by the original model resulted from the overestimated soil temperature for the alpine wetlands. Firstly,

389 as the presence of ice could impede the water movement, the water lateral flows were promoted by the original model due to
 390 the neglecting of freeze-thaw cycles. These further resulted in the lower simulated soil moisture as compared with the
 391 modified model (Fig. S5), which provided favorable oxygen conditions for N₂O production. Meanwhile, the simulated high
 392 soil moisture by the modified model provided feasible anaerobic conditions for thoroughly denitrification. Secondly, higher
 393 simulated soil temperature by the original model also facilitated the mineralization, which provided more available mineral
 394 nitrogen. Field studies showed that high SOC concentrations could stimulate the processes of mineralization and nitrification
 395 in the forests (e.g., Li *et al.*, 2005; Yao *et al.*, 2019). The model input of soil organic matter measured in the observed alpine
 396 forests was more than twice that in the observed alpine meadows (Table S3). Thus, the high SOC content at the alpine forest
 397 site provided more available nitrogen through mineralization and thus stimulated the nitrification processes in the simulation.
 398 Furthermore, the seasonal grazing that occurred in the alpine meadows resulted in constant loss of available nitrogen and
 399 thus hindered the N₂O emissions from the biological processes in the simulation. Field observations showed that the soil
 400 freeze-thaw cycles occurred in seasonally frozen regions not only increased the availability of nitrogen and carbon substrates
 401 by disrupting of soil aggregates but also affected the structure, population and activity of the microbes, and thus influencing
 402 the emissions of N₂O (e.g., Song *et al.*, 2019). de Bruijn *et al.* (2009) have explored the combined mechanisms for
 403 simulating freeze-thaw related N₂O emissions, which were the promoted anaerobiosis and denitrification due to reduced gas
 404 diffusion derived from soil frost and snow cover, and the stimulated microbial growth due to easy decomposable organic
 405 carbon and nitrogen derived from the dead microbes during freeze-thaw cycles. Wolf *et al.* (2011) introduced an impedance
 406 factor to parameterize the reduced water flow between layers in the presence of ice, which could captured the freeze-thaw
 407 related N₂O emissions for ungrazed steppe. In the CNMM-DNDC, threshold values of soil temperature were set to trigger
 408 the death of microbes during the freezing period and stimulate the production of NO, N₂O and N₂ using substrates derived
 409 from the dead microbes during the thawing period, which was similar to one of the mechanisms explored by de Bruijn *et al.*
 410 (2009). However, compared with the simulated freeze-thaw related N₂O emissions by other studies, the simulated dynamics
 411 of peak emissions due to freeze-thaw cycles in this study were inconsistent with those from the field observations. Thus,
 412 improvements are required to incorporate some other effective mechanisms to better capture the dynamic characteristics. The
 413 peak emissions during the freeze-thaw period were not captured by the original model due to the significantly overestimated
 414 soil temperature. The low evaluation statistics for the daily fluxes, especially for the alpine forests, were also attributed to the
 415 underestimation of background emissions, which resulted from both measurement errors due to low fluxes around detection
 416 limits ($\pm 0.41 \text{ g N ha}^{-1} \text{ d}^{-1}$) and model deficiencies in the simulation of tight nitrogen cycling in natural ecosystems.

417 Compared with the empirical model, one key advantage of the process-oriented models is that the models are
 418 independent of the local parameterization (Zhang *et al.*, 2015). In this study, default internal parameter combinations of
 419 biogeochemical processes were used for the original and modified models, which have been applied in the catchment
 420 simulation in the subtropical region (Zhang *et al.*, 2018b), due to the limited field observations (only one year) for both
 421 calibration and validation. The biogeochemical processes were predicted by the first-order and Michaelis-Menten kinetics in
 422 the CNMM-DNDC based on some defined parameters of flow fractionation. For instance, there are 17 parameters related

with N₂O emission in the module of denitrification (Table S6), which would inevitably increase the uncertainty of simulation. Houska *et al.* (2017) found that hydro-biogeochemical models can be right for the wrong reasons, such as matching greenhouse gas emissions while failing to simulate soil moisture, which emphasized the importance for simultaneous validations of multi-variables. Thus, simultaneous validations of CH₄ and N₂O fluxes, as well as soil environment variables, were necessary for comprehensive evaluation of the model performance. In addition, the microbial ecology was recently recommended to be integrated into the biogeochemical model using a smaller number of well-defined kinetic parameters, such as MOMOS (Pansu *et al.*, 2010; Treseder *et al.*, 2011). Therefore, direct control of microbial on biogeochemical processes, such as the stoichiometry of decomposer, is required to be included in the CNMM-DNDC in near future. The model performances of simulating various variables for three typical alpine ecosystems in the Rierlangshan catchment imply that the modified CNMM-DNDC can be applied to predict the thermal dynamics and fluxes of CH₄ and N₂O from alpine ecosystems in seasonally frozen regions.

4.4 Implications for degraded alpine ecosystems

The typical natural wetland alpine ecosystems, which are annually inundated, act as greenhouse gas sinks or are neutral (e.g., Cai., 2012; Tan *et al.*, 2020). A previous study showed that more than 90% of the annually inundated wetlands on the Tibetan Plateau have been degraded and become seasonally inundated or wet alpine meadows due to intentional drainage for grazing since the 1960s (Wei *et al.*, 2015). Zhang *et al.* (2019) found that annual CH₄ emissions from permanently inundated wetlands were 7.1 times higher than those from degraded wetlands with seasonal inundation. Assuming N₂O emissions were zero for permanently inundated wetlands (e.g., Kolb and Horn, 2012; Hatano, 2019), the aggregate emissions of CH₄ and N₂O were estimated at 10.8 Mg CO₂eq ha⁻¹ yr⁻¹ for natural alpine wetlands based on observations used for model validation in this study, which were higher than the scenario simulation. Both the observations and simulations showed that in comparison to annually inundated wetlands, wetland degradation stimulated N₂O emissions to a small extent but reduced CH₄ emissions to a large extent. Thus, compared to that from natural wetlands, the aggregate emissions of CH₄ and N₂O from degraded wetlands were largely reduced but still higher than those of adjacent wet alpine meadows. These results were consistent with the field observations of CH₄ and N₂O emissions along different water table transects in the Zoige peatland, which were primarily driven by soil water content and SOC (Zhang *et al.*, 2020). The decline in the water table resulted in recessive succession of the vegetation for the Zoige wetland with a typical mode of marsh, marsh meadow and meadow (Xiang *et al.*, 2009). Thus, one may deduce that the degradation of annually inundated wetlands at a large-scale might have greatly reduced the aggregate emissions of CH₄ and N₂O from the Zoige wetland, especially for CH₄. However, a recent meta-analysis showed that the reduction in the aggregate emissions of CH₄ and N₂O for the degraded wetlands may be completely offset by the decreased net CO₂ uptake (Tan *et al.*, 2020). For natural wetlands, anaerobic conditions under high a water table inhibit litter decomposition, and thus, a large amount of organic matter is sequestered (Nahlik and Fennessy, 2016). When the annually inundated wetlands degrade to seasonally inundated wetlands or meadows, the rate of peat soil oxidation is enhanced, thus significantly increasing ecosystem respiration and resulting in a

shift from net sinks of greenhouse gas emissions to notable sources (Tan *et al.*, 2020). Consistent with the results of the meta-analysis, the simulation showed that the loss rate of SOC (consisting of microbes, humads and humus) was much higher for degraded wetlands than for other typical alpine ecosystems. These results also indicate the large risk of soil carbon loss, which has been sequestered since the Last Glacial Maximum. The simulation by the modified CNMM-DNDC showed that the model has the potential to simulate hydro-biogeochemical processes in seasonally frozen regions for various alpine ecosystems.

5 Conclusions

To apply the process-oriented hydro-biogeochemical model Catchment Nutrient Management Model - DeNitrification-DeComposition (CNMM-DNDC) in seasonally frozen regions, an improved module of soil thermal dynamics for describing the soil thermal regime in the presence of freeze-thaw cycles was incorporated in this study. Using the unique experimental dataset obtained in the Rierlangshan catchment with the typical alpine wetland, meadow and forest ecosystems, the modified model was evaluated for simulating soil thermal dynamics (soil profile temperature), topsoil moisture and methane (CH₄) and nitrous oxide (N₂O) fluxes for the three ecosystems and the effects of wetland degradation on CH₄ and N₂O fluxes in seasonally frozen regions of the Tibetan Plateau. The modified CNMM-DNDC could generally captured the seasonal dynamics and magnitudes of profile soil temperature, topsoil moisture and fluxes of CH₄ and N₂O in seasonally frozen regions and showed the potential to simulate the impacts of wetland degradation on the fluxes of CH₄ and N₂O. Both the observed and simulated CH₄ and N₂O fluxes from alpine wetlands and meadows, as well as the results from the simulated annually inundated wetlands, indicate that wetland degradation resulted in a significant reduction in the aggregate emissions of CH₄ and N₂O. Reduced soil moisture was the key factor for the decreased aggregate emissions of CH₄ and N₂O which were primarily determined by the CH₄ emissions. This study implies that a hydro-biogeochemical model, such as the modified CNMM-DNDC, are able to predict soil thermal dynamics, topsoil moisture and fluxes of CH₄ and N₂O in seasonally frozen regions with an improved physical-based soil thermal module.

Data availability

The model, input and output databases can be obtained from the first author and all the observed data sets used in this study can be available from the co-authors.

Author contribution

Zheng, X. and Zhang, W. contributed to developing the idea and enhancing the science of this study. Zhang, W. improved the scientific processes of the model, implemented the model simulations and prepared the manuscript with contributions

484 from all co-authors. Li, S. improved the model structure for standard input. Yao, Z., Zhang, H., Ma, L., Wang, K., Wang, R.
485 and Liu, C. designed and carried out the field experiments. Han, S. collected and established the input database for modelling.
486 Deng, J and Li, Y contributed to the modification of the model and the improvement of the manuscript.

487 **Competing interests**

488 The authors declare that they have no conflict of interest.

489 **Acknowledgement**

490 This study was jointly supported by the National Key R&D Program of China (2016YFA0602303), the Chinese Academy of
491 Sciences (ZDBS-LY-DQC007), the National Key Scientific and Technological Infrastructure project “Earth System Science
492 Numerical Simulator Facility” (EarthLab) and the National Natural Science Foundation of China (41603075, 41861134029).

493 **References**

- 494 Bechmann, M., 2014. Long-term monitoring of nitrogen in surface and subsurface runoff from small agricultural dominated
495 catchments in Norway. *Agric. Ecosyst. Environ.* 198, 13–24.
- 496 Bosch, N., Allan, J., Dolan, D., Han, H., Richards, R., 2011. Application of the Soil and Water Assessment Tool for six
497 watersheds of Lake Erie: Model parameterization and calibration. *J. Great Lakes Res.* 37, 263–271.
- 498 Breuer, L., VachÉ, K., Julich, S., Frede, H., 2010. Current concepts in nitrogen dynamics for mesoscale catchments. *Hydrol.*
499 *Sci. J.-J. Sci. Hydrol.* 53, 1059–1074.
- 500 Canfield, D., Glazer, A., Falkowski, P., 2010. The evolution and future of Earth's nitrogen cycle. *Science* 330, 192–196.
- 501 Cai, Z., 2012. Greenhouse gas budget for terrestrial ecosystems in China. *Sci. China-Earth Sci.* 55, 173–182.
- 502 Castellano, M., Lewis, D., Kaye, J., 2013. Response of soil nitrogen retention to the interactive effects of soil texture,
503 hydrology, and organic matter. *J. Geophys. Res.-Biogeosci.* 118, 280–290.
- 504 Chen, D., Li, Y., Grace, P., Mosier, A., 2008. N₂O emissions from agricultural lands: a synthesis of simulation approaches.
505 *Plant Soil* 309, 169–189.
- 506 Cheng, K., Ogle, S., Parton, W., Pan, G., 2014. Simulating greenhouse gas mitigation potentials for Chinese Croplands using
507 the DAYCENT ecosystem model. *Glob. Change Biol.* 20, 948–962.
- 508 Collatz, G., Ribas-Carbo, M., Berry, J., 1992. Coupled photosynthesis-stomatal conductance model for leaves of C₄ plants,
509 *Aust. J. Plant Physiol.*, 19, 519–538.
- 510 Collins, A., Zhang, Y., Winter, M., Inman, A., Jones, J., Johnes, P., Cleasby, W., Vrain, E., Lovett, A., Noble, L., 2016.
511 Tackling agricultural diffuse pollution: What might uptake of farmer-preferred measures deliver for emissions to water
512 and air? *Sci. Total Environ.* 547, 269–281.
- 513 Congreves, K., Grant, B., Dutta, B., Smith, W., Chantigny, M., Rochette, Desjardins, R., 2016. Prediction ammonia
514 volatilization after field application of swine slurry: DNDC model development, *Agric. Ecosyst. Environ.* 219, 179–189.
- 515 Cui, Z., Zhang, H., Chen, X., Zhang, C., Ma, W., Huang, C., Zhang, W., Mi, G., Miao, Y., Li, X., Gao, Q., Yang, J., Wang,
516 Z., Ye, Y., Guo, S., Lu, J., Huang, J., Lv, S., Sun, Y., Liu, Y., Peng, X., Ren, J., Li, S., Deng, X., Shi, X., Zhang, Q.,
517 Yang, Z., Tang, L., Wei, C., Jia, L., Zhang, J., He, M., Tong, Y., Tang, Q., Zhong, X., Liu, Z., Cao, N., Kou, C., Ying,
518 H., Yin, Y., Jiao, X., Zhang, Q., Fan, M., Jiang, R., Zhang, F., Dou, Z., 2018. Pursuing sustainable productivity with
519 millions of smallholder farmers. *Nature* 555, 363–366.

520 Cui, F., Zheng, X., Liu, C., Wang, K., Zhou, Z., Deng, J., 2014. Assessing biogeochemical effects and best management
521 practice for a wheat-maize cropping system using the DNDC model. *Biogeosciences* 11, 91–107.

522 Cuo, L., Zhang, Y., Bohn, T., Zhao, L., Li, J., Liu, Q., Zhou, B., 2015. Frozen soil degradation and its effects on surface
523 hydrology in the northern Tibetan Plateau. *J. Geophys. Res. Atmos.* 120, 8276–8298.

524 de Bruijn, A.M.G., Butterbach-Bahl, K., Blagodatsky, S., Grote, R., 2009. Model evaluation of different mechanisms driving
525 freeze–thaw N₂O emissions. *Agric. Ecosyst. Environ.* 133, 196–207.

526 Deng, J., Li, C., Frolking, S., Zhang, Y., Bäckstrand, K., Crill, P., 2014. Assessing effects of permafrost thaw on C fluxes
527 based on multiyear modeling across a permafrost thaw gradient at Stordalen, Sweden. *Biogeosciences* 11, 4753–4770.

528 Dong, Z., Hu, G., Yan, C., Wang, W., Lu, J., 2010. Aeolian desertification and its causes in the Zoige Plateau of China's
529 Qinghai–Tibetan Plateau. *Environ. Earth Sci.* 59, 1731–1740.

530 Dubache, G., Li, S., Zheng, X., Zhang, W., Deng, J., 2019. Modeling ammonia volatilization following urea application to
531 winter cereal fields in the United Kingdom by improving a biogeochemical model, *Sci. Total Environ.* 660, 1403–1418.

532 Farquhar, G., Caemmerer, S., Berry, J., 1980. A biochemical model of photosynthetic CO₂ assimilation in leaves of C₃
533 species. *Planta*, 149, 78–90.

534 Fenner, N., Freeman, C., 2011. Drought-induced carbon loss in peatlands. *Nat. Geosci.* 4, 895–900.

535 Foereid, B., Barthram, G., Marriott, C., 2007. The CENTURY model failed to simulate soil organic matter development in
536 an acidic grassland. *Nutr. Cycl. Agroecosyst.* 78, 143–153.

537 Ford, T., Harris, E., Quiring, S., 2014. Estimating root zone soil moisture using near-surface observations from SMOS.
538 *Hydrol. Earth Syst. Sci.* 18, 139–154.

539 Galloway, J., Dentener, F., Capone, D., Boyer, E., Howarth, R., Seitzinger, S., Asner, G., Cleveland, C., Green, P., Holland,
540 E., Karl, D., Michaels, A., Porter, J., Townsend, A., Vorosmarty, C., 2004. Nitrogen Cycles: past, present, and future.
541 *Biogeochemistry* 70, 153–226.

542 Galloway, J., Townsend, A., Erisman, J., Bekunda, M., Cai, Z., Freney, J., Martinelli, L., Seitzinger, S., Sutton, M., 2008.
543 Transformation of the nitrogen cycle: recent trends, questions, and potential solutions. *Science* 320, 889–892.

544 Giltrap, D.L., Li, C., Saggar, S., 2010. DNDC: A process-based model of greenhouse gas fluxes from agricultural soils.
545 *Agric. Ecosyst. Environ.* 136, 292–300.

546 Gong, Y., Wu, J., Vogt, J., Ma, W., 2020. Greenhouse gas emissions from peatlands under manipulated warming, nitrogen
547 addition, and vegetation composition change: a review and data synthesis. *Environ. Rev.* 28, 428–437.

548 Haas, E., Klatt, S., Fröhlich, A., Kraft, P., Werner, C., Kiese, R., Grote, R., Breuer, L., Butterbach-Bahl, K., 2012.
549 LandscapeDNDC: a process model for simulation of biosphere–atmosphere–hydrosphere exchange processes at site and
550 regional scale. *Landsc. Ecol.* 28, 615–636.

551 Hatano, R., 2019. Impact of land use change on greenhouse gases emissions in peatland: a review. *Int. Agrophys.* 33, 167–
552 173.

553 Holzworth, D., Huth, N., deVoil, P., Zurcher, E., Herrmann, N., McLean, G., Chenu, K., van Oosterom, E., Snow, V.,
554 Murphy, C., Moore, A., Brown, H., Whish, J., Verrall, S., Fainges, J., Bell, L., Peake, A., Poulton, P., Hochman, Z.,
555 Thorburn, P., Gaydon, D., Dalgliesh, N., Rodriguez, D., Cox, H., Chapman, S., Doherty, A., Teixeira, E., Sharp, J.,
556 Cichota, R., Vogeler, I., Li, F., Wang, E., Hammer, G., Robertson, M., Dimes, J., Whitbread, A., Hunt, J., van Rees, H.,
557 McClelland, T., Carberry, P., Hargreaves, J., MacLeod, N., McDonald, C., Harsdorf, J., Wedgwood, S., Keating, B.,
558 2014. APSIM – Evolution towards a new generation of agricultural systems simulation. *Environ. Modell. Softw.* 62,
559 327–350.

560 Houska, T., Kraus, D., Kiese, R., Breuer, L., 2017. Constraining a complex biogeochemical model for CO₂ and N₂O
561 emission simulations from various land uses by model–data fusion. *Biogeosciences* 14, 3487–3508.

562 Huang, C., 2000. *Soil Science*. China Agriculture Press, Beijing. Pp. 125. (In Chinese)

563 Hugelius, G., Loisel, J., Chadburn, S., Jackson, R., Jones, M., MacDonald, G., Marushchak, M., Olefeldt, D., Maara, P.,
564 Siewert, M., Treat, C., Turetsky, M., Voigt, C., Yu, Z., 2020. Large stocks of peatland carbon and nitrogen are
565 vulnerable to permafrost thaw. *Proc. Natl. Acad. Sci. U. S. A.* doi: 10.1073/pnas.1916387117

566 Intergovernmental Panel on Climate Change (IPCC): Climate Change 2013: The Physical Science Basis, Contribution of
567 Working Group I to the Fifth Assessment Report of the Intergovernmental Panel on Climate Change (eds. Stocker TF,
568 Qin D, Plattner G-K, et al.), Cambridge University Press, Cambridge, United Kingdom and New York, NY, USA, 2013.

569 Jiang, H., Yi, Y., Zhang, W., Yang, K., Chen, D., 2020. Sensitivity of soil freeze/thaw dynamics to environmental conditions
570 at different spatial scales in the central Tibetan Plateau. *Sci. Total Environ.* 734, 139261. doi:
571 org/10.1016/j.scitotenv.2020.139261

572 Jiang, Z., 2010. Analysis on the establishment conditions of the square sum decomposition formular of regression model, *J.*
573 *Industr. Techn. Econ.* 29(4), 116–119 (in Chinese).

574 Johansen, O., 1975. Thermal conductivity of soils. Ph.D. thesis, Univ. of Trondheim, Trondheim, Norway.

575 Ju, X., Xing, G., Chen, X., Zhang, S., Zhang, L., Liu, X., Cui, Z., Yin, B., Christie, P., Zhu, Z., Zhang, F., 2009. Reducing
576 environmental risk by improving N management in intensive Chinese agricultural systems. *Proc. Natl. Acad. Sci. U.*
577 *S. A.* 106, 3041–3046.

578 Kandel, T., Lærke, P., Elsgaard, L., 2018. Annual emissions of CO₂, CH₄ and N₂O from a temperate peat bog: comparison of
579 an undrained and four drained sites under permanent grass and arable crop rotations with cereals and potato. *Agric. For.*
580 *Meteorol.* 256–257, 470–481.

581 Kang, X., Li, Y., Wang, J., Yan, L., Zhang, X., Wu, H., Yan, Z., Zhang, K., Hao, Y., 2020. Precipitation and temperature
582 regulate the carbon allocation process in alpine wetlands: quantitative simulation. *J. Soils Sediments* 20, 3300–3315.

583 Keiluweit, M., Wanzek, T., Kleber, M., Nico, P., Fendorf, S., 2017. Anaerobic microsites have an unaccounted role in soil
584 carbon stabilization. *Nat. Commun.* 8. doi: 10.1038/s41467-017-01406-6

585 Klatt, S., Kraus, D., Kraft, P., Breuer, L., Wlotzka, M., Heuveline, V., Haas, E., Kiese, R., Butterbach-Bahl, K., 2017.
586 Exploring impacts of vegetated buffer strips on nitrogen cycling using a spatially explicit hydro-biogeochemical
587 modeling approach. *Environ. Modell. Softw.* 90, 55–67.

588 Kolb, S., Horn, M., 2012. Microbial CH₄ and N₂O consumption in acidic wetlands. *Front. Microbiol.* 3, 78. doi:
589 10.3389/fmicb.2012.00078

590 Li, B., Yu, Z., Liang, Z., Song, K., Li, H., Wang, Y., Zhang, W., Acharya, K., 2014. Effects of climate variations and human
591 activities on runoff in the Zoige alpine wetland in the eastern edge of the Tibetan Plateau. *J. Hydrol. Eng.* 19, 1026–
592 1035.

593 Li, C., 2000. Modeling trace gas emissions from agricultural ecosystems. *Nutr. Cycl. Agroecosyst.* 58, 259–276.

594 Li, C., 2007. Quantifying greenhouse gas emissions from soils: scientific basis and modeling approach. *Soil Sci. Plant Nutr.*
595 53, 344–352.

596 Li, C., 2016. Biogeochemistry: Scientific Fundamentals and Modelling Approach. Tsinghua University Press, Beijing. Pp.
597 530. (In Chinese)

598 Li, C., Frolking, S., Butterbach-Bahl, K., 2005. Carbon sequestration in arable soils is likely to increase nitrous oxide
599 emissions, offsetting reductions in climate radiative forcing. *Clim. Change* 72, 321–338.

600 Li, S., Zheng, X., Zhang, W., Han, S., Deng, J., Wang, K., Wang, R., Yao, Z., Liu, C., 2019. Modeling ammonia
601 volatilization following the application of synthetic fertilizers to cultivated uplands with calcareous soils using an
602 improved DNDC biogeochemistry model. *Sci. Total Environ.* 660, 931–946.

603 Li, Y., White, R., Chen, D., Zhang, J., Li, B., Zhang, Y., Huang, Y., Edis, R., 2007. A spatially referenced water and
604 nitrogen management model (WNMM) for (irrigated) intensive cropping systems in the North China Plain. *Ecol. Model.*
605 203, 395–423.

606 Liu, C., Holst, J., Brüggemann, N., Butterbach-Bahl, K., Yao, Z., Yue, J., Han, S., Han, X., Krümmelbein, J., Horn, R.,
607 Zheng, X., 2007. Winter-grazing reduces methane uptake by soils of a typical semi-arid steppe in Inner Mongolia,
608 China. *Atmos. Environ.* 41, 5948–5958.

609 Liu, S., Xie, Z., Zeng, Y., Liu, B., Li, R., Wang, Y., Wang, L., Qin, P., Jia, B., Xie, J., 2019. Effects of anthropogenic
610 nitrogen discharge on dissolved inorganic nitrogen transport in global rivers. *Glob. Change Biol.* 25, 1493–1513.

611 Ma, L., Yao, Z., Zheng, X., Zhang, H., Wang, K., Zhu, B., Wang, R., Zhang, W., Liu, C., 2018. Increasing grassland
612 degradation stimulates the non-growing season CO₂ emissions from an alpine meadow on the Qinghai-Tibetan Plateau.
613 *Environ. Sci. Pollut. Res.* 25, 26576–26591.

614 McClain, M., Boyer, E., Dent, C., Gergel, S., Grimm, N., Groffman, P., Hart, S., Harvey, J., Johnston, C., Mayorga, E., 2003.
615 Biogeochemical hot spots and hot moments at the interface of terrestrial and aquatic ecosystems. *Ecosystems* 6, 301–
616 312.

617 Moriasi, D., Arnold, J., Van Liew, M., Bingner, R., Harmel, R., Veith, T., 2007. Model evaluation guidelines for systematic
618 quantification of accuracy in watershed simulation, *T. Am. Soc. Agr. Biol. Eng.* 50, 885–900.

619 Nahlik, A., Fennessy, M., 2016. Carbon storage in US wetlands. *Nat. Commun.* 7, 13835. doi: 10.1038/ncomms13835

620 Nash, J., Sutcliffe, J., 1970. River flow forecasting through conceptual models: part I- a discussion of principles, *J. Hydrol.*

621 10, 282–290.

622 Pansu, M., Sarmiento, L., Rujano, M., Ablan, M., Acevedo, D., Bottner, P., 2010. Modelling Organic transformations by

623 Micro-Organisms of Soils in six contrasting ecosystems: validation of the MOMOS model. *Glob. Biogeochem. Cycl.* 24,

624 GB1008. doi: org/10.1029/2009GB003527

625 Pansu, M., Machado, D., Bottner, P., Sarmiento, L., 2014. Modelling microbial exchanges between forms of soil nitrogen in

626 contrasting ecosystems. *Biogeosciences* 11, 915–927.

627 Piao, S., Fang, J., Ciais, P., Peylin, P., Huang, Y., Sitch, S., Wang, T., 2009. The carbon balance of terrestrial ecosystems in

628 China. *Nature* 458, 1009–1013.

629 Pohlert, T., Huisman, J., Breuer, L., Frede, H., 2007. Integration of a detailed biogeochemical model into SWAT for

630 improved nitrogen predictions—Model development, sensitivity, and GLUE analysis. *Ecol. Model.* 203, 215–228.

631 Pollack, H., Chapman, D., 1977. On the regional variation of heat flow, geotherms, and lithospheric thickness.

632 *Tectonophysics* 38, 279–296.

633 Schroeck, A., Gaube, V., Haas, E., Winiwarter, W., 2019. Estimating nitrogen flows of agricultural soils at a landscape level

634 - A modelling study of the Upper Enns Valley, a long-term socio-ecological research region in Austria. *Sci. Total*

635 *Environ.* 665, 275–289.

636 Schuur, E., McGuire, A., Schadel, C., Grosse, G., Harden, J., Hayes, D., Hugelius, G., Koven, C., Kuhry, P., Lawrence, D.,

637 Natali, S., Olefeldt, D., Romanovsky, V., Schaefer, K., Turetsky, M., Treat, C., Vonk, J., 2015. Climate change and the

638 permafrost carbon feedback. *Nature* 520, 171–179.

639 Seitzinger, S., 2008. Nitrogen cycle - Out of reach. *Nature* 452, 162–163.

640 Song, L., Yao, Y., Lin, L., Gao, W., Cai, T., Liang, H., Gao, D., 2019. The potential source of nitrous oxide in the pristine

641 riparian marsh during freeze-thaw cycles, case study in Northeast China. *Ecol. Eng.* 134, 18–25.

642 Tan, L., Ge, Z., Zhou, X., Li, S., Li, X., Tang, J., 2020. Conversion of coastal wetlands, riparian wetlands, and peatlands

643 increases greenhouse gas emissions: a global meta-analysis. *Glob. Change Biol.* 26, 1638–1653.

644 Todd-Brown, K., Hopkins, F., Kivlin, S., Jennifer, M., Talbot, J., Allison, S., 2012. A framework for representing microbial

645 decomposition in coupled climate models. *Biogeochemistry* 109, 19–33.

646 Treseder, K., Balser, T., Bradford, M., Brodie, E., Dubinsky, E., Eviner, V., Hofmockel, K., Lennon, J., Levine, U.,

647 MacGregor, B., Pett-Ridge, J., Waldrop, M., 2011. Integrating microbial ecology into ecosystem models: challenges

648 and priorities. *Biogeochemistry* 109, 7–18.

649 Vereecken, H., Schnepf, A., Hopmans, J., Javaux, M., Or, D., Roose, T., Vanderborght, J., Young, M., Amelung, W.,

650 Aitkenhead, M., Allison, S., Assouline, S., Baveye, P., Berli, M., Brüggemann, N., Finke, P., Flury, M., Gaiser, T.,

651 Govers, G., Ghezzehei, T., Hallett, P., Hendricks Franssen, H., Heppell, J., Horn, R., Huisman, J., Jacques, D., Jonard,

652 F., Kollet, S., Lafolie, F., Lamorski, K., Leitner, D., McBratney, A., Minasny, B., Montzka, C., Nowak, W., Pachepsky,

653 Y., Padarian, J., Romano, N., Roth, K., Rothfuss, Y., Rowe, E., Schwen, A., Šimůnek, J., Tiktak, A., Van Dam, J., van

654 der Zee, S., Vogel, H., Vrugt, J., Wöhling, T., Young, I., 2016. Modeling Soil Processes: Review, Key Challenges, and

655 New Perspectives. *Vadose Zone J.* 15, doi:10.2136/vzj2015.2009.0131.

656 Wania, R., Ross, I., Prentice, I., 2009. Integrating peatlands and permafrost into a dynamic global vegetation model: 1.

657 Evaluation and sensitivity of physical land surface processes. *Glob. Biogeochem. Cycl.* 23, GB3014,

658 doi:10.1029/2008GB003412.

659 Wei, D., Xu-Ri, T., Tarchen, T., Dai, D., Wang, Y., Wang, Y., 2015. Revisiting the role of CH₄ emissions from alpine wetlands

660 on the Tibetan Plateau: evidence from two in situ measurements at 4758 and 4320 m above sea level. *J. Geophys. Res.-*

661 *Biogeosci.* 120, 1741–1750.

662 Wigmosta, M., Vail, L., Lettenmaier, D., 1994. A distributed hydrology-vegetation model for complex terrain. *Water Resour.*

663 *Res.*, 30, 1665–1679.

664 Willmott, C., Matsuura, K., 2005. Advantages of the mean absolute error (MAE) over the root mean square error (RMSE)

665 in assessing average model performance, *Clim. Res.*, 30, 79–82.

666 Wolf, B., Kiese, R., Chen, W., Grote, R., Zheng, X., Butterbach-Bahl, K., 2011. Modelling N₂O emissions from steppe in

667 Inner Mongolia, China, with consideration of spring thaw and grazing intensity. *Plant Soil* 350, 297–310.

Wu, Y., Liu, S., Qiu, L., Sun, Y., 2016. SWAT-DayCent coupler: An integration tool for simultaneous hydro-biogeochemical modeling using SWAT and DayCent. *Environ. Modell. Softw.* 86, 81–90.

Xiang, S., Guo, R., Wu, N., Sun, S., 2009. Current status and future prospects of Zoige Marsh in Eastern Qinghai-Tibet Plateau. *Ecol. Eng.* 35, 553–562.

Yao, Z., Ma, L., Zhang, H., Zheng, X., Wang, K., Zhu, B., Wang, R., Wang, Y., Zhang, W., Liu, C., Butterbach-Bahl, K., 2019. Characteristics of annual greenhouse gas flux and NO release from alpine meadow and forest on the eastern Tibetan Plateau. *Agric. For. Meteorol.* 272–273, 166–175.

Zhang, H., Yao, Z., Ma, L., Zheng, X., Wang, R., Wang, K., Liu, C., Zhang, W., Zhu, B., Tang, X., Hu, Z., Han, S., 2019. Annual methane emissions from degraded alpine wetlands in the eastern Tibetan Plateau. *Sci. Total Environ.* 657, 1323–1333.

Zhang, H., Yao, Z., Wang, K., Zheng, X., Ma, L., Wang, R., Liu, C., Zhang, W., Zhu, B., Tang, X., Hu, Z., Han, S., 2018a. Annual N₂O emissions from conventionally grazed typically alpine grass meadows in the eastern Qinghai-Tibetan Plateau. *Sci. Total Environ.* 625, 885–899.

Zhang, W., Li, Y., Zhu, B., Zheng, X., Liu, C., Tang, J., Su, F., Zhang, C., Ju, X., Deng, J., 2018b. A process-oriented hydro-biogeochemical model enabling simulation of gaseous carbon and nitrogen emissions and hydrologic nitrogen losses from a subtropical catchment. *Sci. Total Environ.* 616–617, 305–317.

Zhang, W., Liu, C., Zheng, X., Fu, Y., Hu, X., Cao, G., Butterbach-Bahl, K., 2014. The increasing distribution area of zokor mounds weaken greenhouse gas uptakes by alpine meadows in the Qinghai-Tibetan Plateau. *Soil Biol. Biochem.* 71, 105–112.

Zhang, W., Liu, C., Zheng, X., Wang, K., Cui, F., Wang, R., Li, S., Yao, Z., Zhu, J., 2019. Using a modified DNDC biogeochemical model to optimize field management of a multi-crop (cotton, wheat, and maize) system: a site-scale case study in northern China. *Biogeosciences* 16, 2905–2922.

Zhang, W., Liu, C., Zheng, X., Zhou, Z., Cui, F., Zhu, B., Haas, E., Klatt, S., Butterbach-Bahl, K., Kiese, R., 2015. Comparison of the DNDC, LandscapedNDC and IAP-N-GAS models for simulating nitrous oxide and nitric oxide emissions from the winter wheat-summer maize rotation system. *Agric. Syst.* 140, 1–10.

Zhang, W., Wang, J., Hu, Z., Li, Y., Yan, Z., Zhang, X., Wu, G., Yan, L., Zhang, K., Kang, X., 2020. The primary drivers of greenhouse gas emissions along the water table gradient in the Zoige alpine peatland. *Water Air Soil Pollut.* 231: 224. doi: [org/10.1007/s11270-020-04605-y](https://doi.org/10.1007/s11270-020-04605-y)

Zhang, Y., Chen, W., Cihlar, J., 2003. A process-based model for quantifying the impact of climate change on permafrost thermal regimes. *J. Geophys. Res.-Atmos.* 108, 4695.

Zhang, Y., Sachs, T., Li, C., Boike, J., 2012. Upscaling methane fluxes from closed chambers to eddy covariance based on a permafrost biogeochemistry integrated model. *Glob. Change Biol.* 18, 1428–1440.

Zhang, Y., Shao, Q., Ye, A., Xing, H., Xia, J., 2016. Integrated water system simulation by considering hydrological and biogeochemical processes: model development, with parameter sensitivity and autocalibration. *Hydrol. Earth Syst. Sci.* 20, 529–553.

Zhu, Q., Castellano, M., Yang, G., 2018. Coupling soil water processes and the nitrogen cycle across spatial scales: potentials, bottlenecks and solutions. *Earth-Sci. Rev.* 187, 248–258.

Zhu, Q., Schmidt, J.P., Bryant, R., 2012. Hot moments and hot spots of nutrient losses from a mixed land use watershed. *J. Hydrol. Eng.* 414, 393–404.

Zhuang, Q., Romanovsk, V., McGuire, A., 2001. Incorporation of a permafrost model into a large-scale ecosystem model: Evaluation of temporal and spatial scaling issues in simulating soil thermal dynamics. *J. Geophys. Res.* 106, 33649–33670.

Zhuang, Q., Melillo, J., Kicklighter, D., Prinn, R., McGuire, A., Steudler, P., Felzer, B., Hu, S., 2004. Methane fluxes between terrestrial ecosystems and the atmosphere at northern high latitudes during the past century: a retrospective analysis with a process-based biogeochemistry model. *Glob. Biogeochem. Cycl.* 18, GB3010, doi:10.1029/2004GB002239.

714

715 Table 1 Statistics of the validated variables by the modified CNMM-DNDC for three typical alpine ecosystems.

716

Item	Ecosystem	n^a	DR ^b	IA O ^c	M ^d	NSE O	M	ZIR-slope O	M	ZIR- R^{2c} O	M	ZIR-P O	M
Soil temperature													
5 cm	Meadow	500	Daily	0.90	0.96	0.82	0.95	0.84	1.09	0.89	0.96	< 0.001	< 0.001
	Forest	48	Daily	0.85	0.91	0.37	0.68	0.64	0.83	0.68	0.73	< 0.001	< 0.001
10 cm	Wetland	366	Daily	0.90	0.98	0.57	0.92	0.72	1.07	0.81	0.93	< 0.001	< 0.001
	Meadow	500	Daily	0.93	0.99	0.71	0.95	0.80	1.08	0.85	0.96	< 0.001	< 0.001
20 cm	Wetland	366	Daily	0.82	0.99	0.18	0.96	0.64	1.05	0.66	0.97	< 0.001	< 0.001
	Meadow	500	Daily	0.87	0.99	0.48	0.97	0.74	1.06	0.76	0.98	< 0.001	< 0.001
50 cm	Wetland	366	Daily	0.66	0.99	-1.01	0.97	0.51	1.05	0.43	0.97	< 0.001	< 0.001
	Meadow	401	Daily	0.70	1.00	-0.48	0.99	0.58	1.06	0.53	1.00	< 0.001	< 0.001
70 cm	Wetland	366	Daily	0.58	0.98	-2.23	0.93	0.47	1.05	0.38	0.93	< 0.001	< 0.001
	Meadow	401	Daily	0.64	1.00	-1.19	0.99	0.54	1.03	0.49	1.00	< 0.001	< 0.001
90 cm	Wetland	366	Daily	0.52	0.98	-4.07	0.90	0.44	1.03	0.36	0.90	< 0.001	< 0.001
Soil moisture	Wetland	74	Weekly	0.63	0.83	-1.65	0.20	1.31	1.13	—	0.60	—	< 0.001
	Meadow	128	Weekly	0.78	0.78	0.28	0.32	0.96	0.93	0.30	0.41	< 0.001	< 0.001
	Forest	40	Weekly	0.48	0.49	-1.04	-0.80	1.21	1.19	—	—	—	—
Daily CH ₄ flux	Wetland	180	Weekly	0.37	0.74	-11.1	-0.73	0.46	0.87	—	—	—	—
	Meadow	168	Weekly	0.87	0.88	0.42	0.38	1.09	0.94	0.44	0.39	< 0.001	< 0.001
	Forest	49	Weekly	0.59	0.57	-2.79	-3.39	0.92	0.79	—	—	—	—
Daily N ₂ O flux	Wetland	180	Weekly	0.01	0.26	-323	-0.07	0.01	0.59	—	—	—	—
	Meadow	168	Weekly	0.23	0.44	-0.16	-1.76	0.99	0.35	—	—	—	—
	Forest	58	Weekly	0.47	0.47	-1.85	-1.64	0.44	0.47	—	—	—	—

717 ^a n indicates the number of the observations. ^b DR denotes the time resolution of the observed data. ^c O indicates the simulations by the original
718 model. ^d M indicates the simulations by the modified model. ^e “—” indicated no value due to the sum of regression square are larger than the sum
719 of the total square for the regression). IA, NSE, ZIR-slope, ZIR- R^2 and ZIR-P indicate the index of agreement, Nash-Sutcliffe index,
720 determination coefficient and slope of the zero-intercept univariate linear regression (ZIR) of the observations against the simulations.

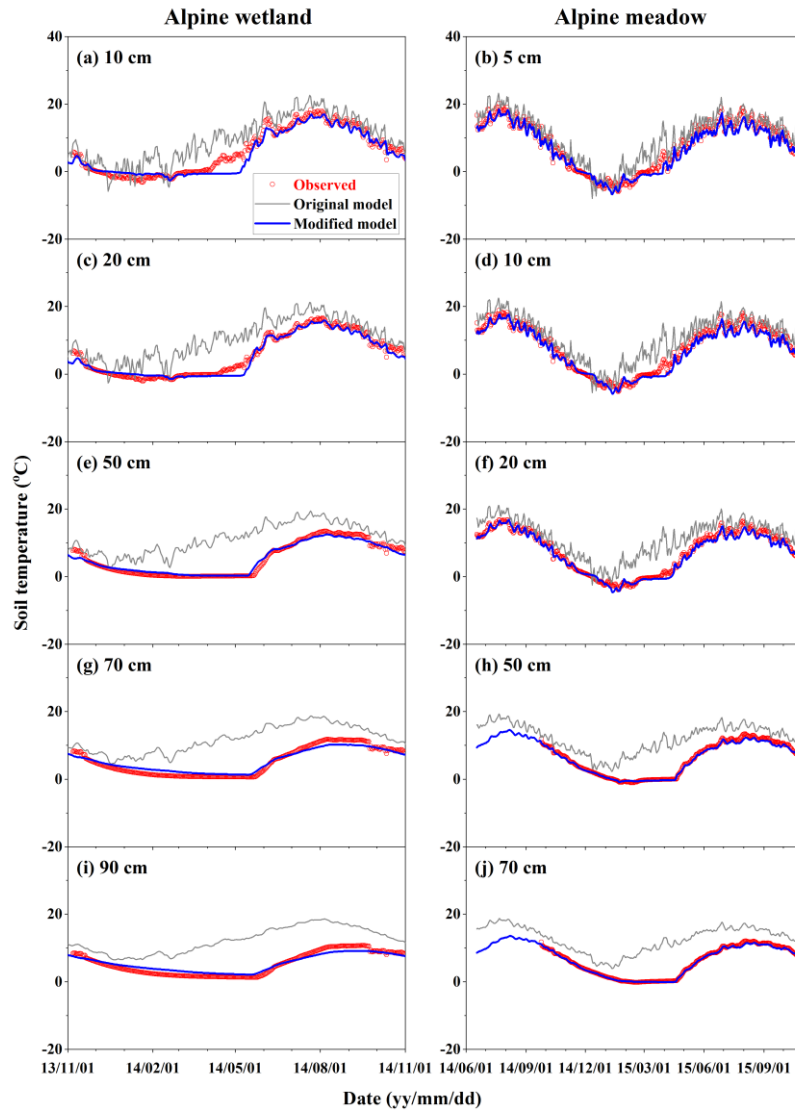


Figure: 1 Observed and simulated daily profile soil temperature from the alpine wetlands and meadows by the original and modified models. The legends in panel a apply for all panels.

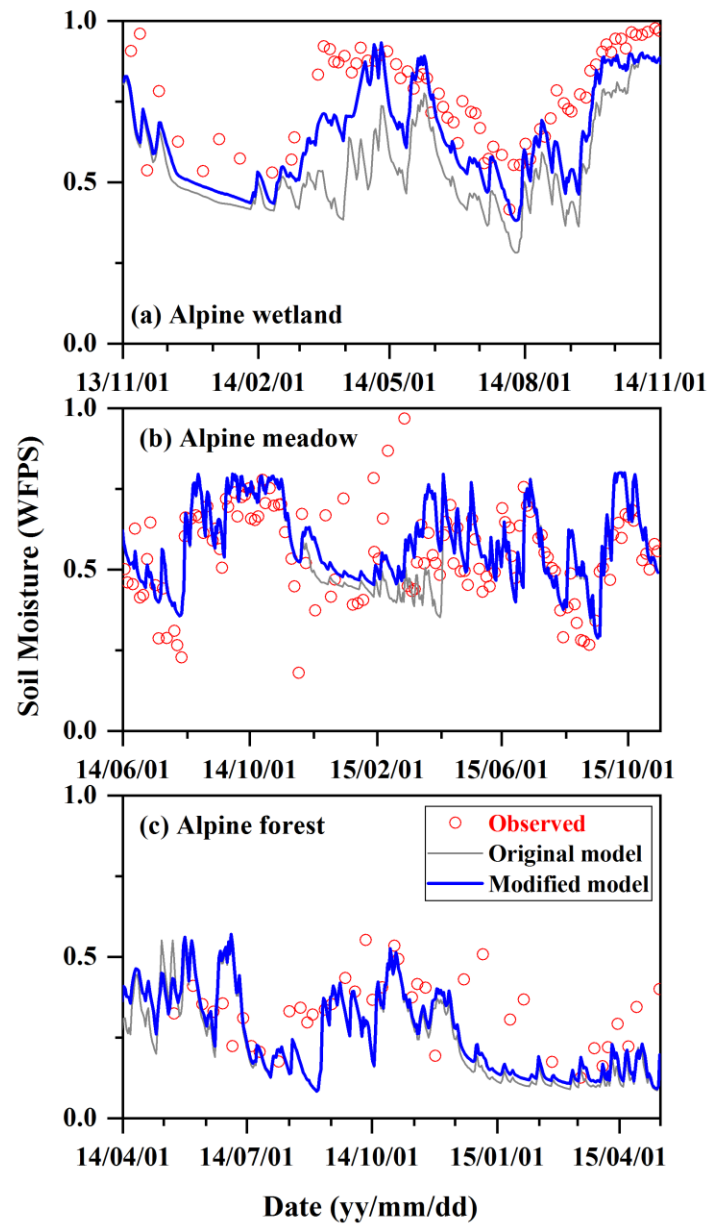


Figure: 2 Observed and simulated daily topsoil (0–6 cm) moisture in the water-filled pore space (WFPS) from the alpine wetlands, meadows and forests by the original and modified models. The legends in panel a apply for all panels.

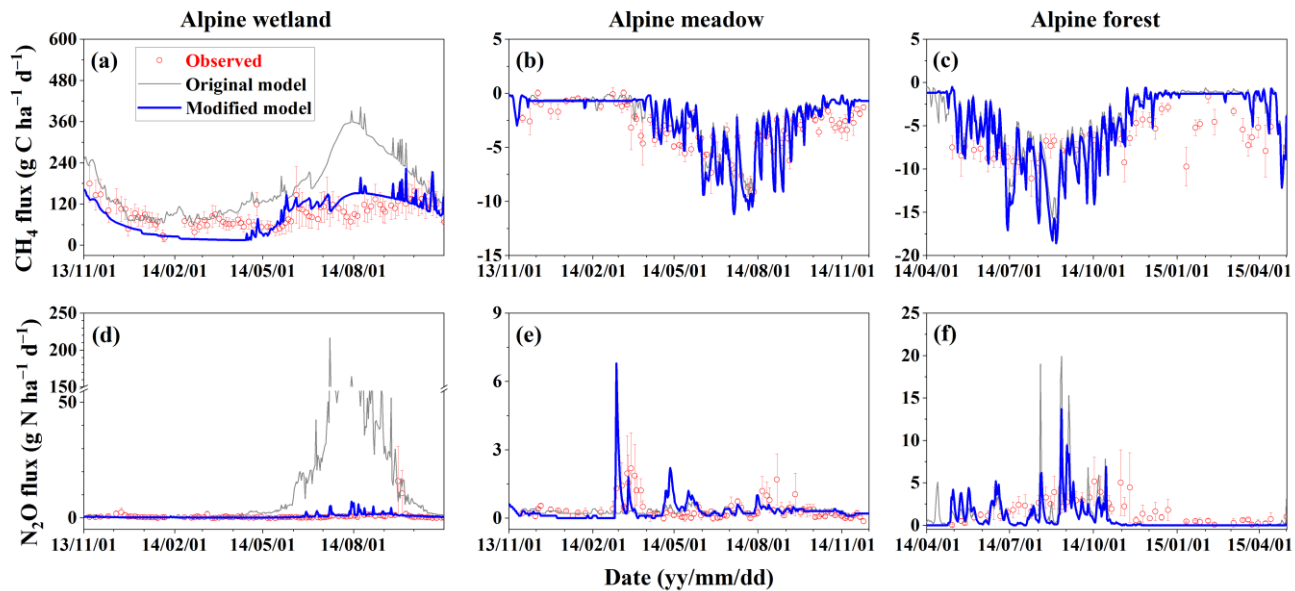
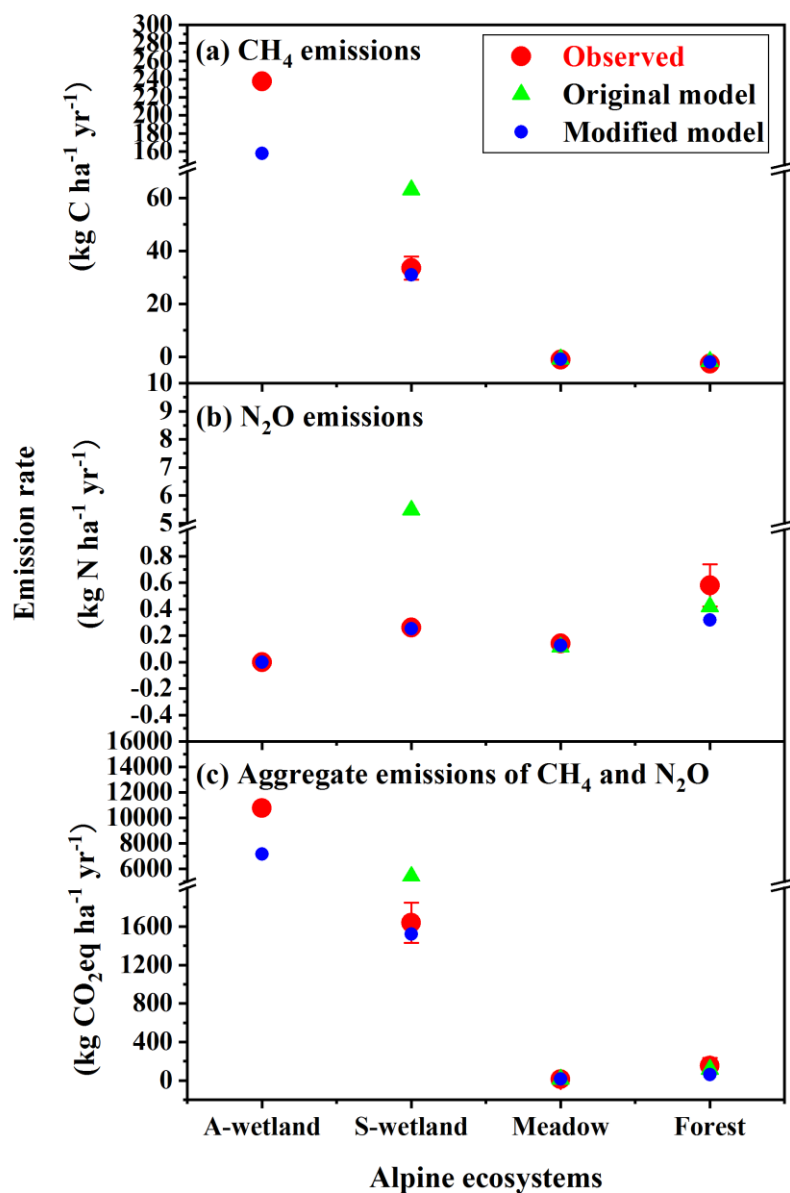


Figure: 3 Observed and simulated daily methane (CH_4) and nitrous oxide (N_2O) fluxes from the alpine wetlands, meadows and forests by the original and modified models. The vertical bar for each observation indicates the standard error of six spatial replicates. The legends in panel a apply for all panels.



731

732 **Figure: 4** Observed and simulated annual emissions of methane (CH₄), nitrous oxide (N₂O) and aggregate emissions of both from
 733 the annually inundated wetlands (A-wetland), seasonally inundated wetlands (S-wetland), alpine meadows and forests. The
 734 legends in panel a apply for all panels.